International Journal of GEOMATE, April, 2022, Vol.22, Issue 92, pp.71-76
ISSN: 2186-2982 (P), 2186-2990 (O), Japan, DOI: https://doi.org/10.21660/2022.92.7560
Geotechnique, Construction Materials and Environment

INFLUENCE OF RAINFALL INTENSITY ON INFILTRATION SURFACE FORMATION OF RIVER EMBANKMENTS

Shin-ichi Kanazawa [1], Tsubasa Ichijo [2] and Hisao Emoto[3]

[1] Civil Engineering Program, Faculty of Engineering, Niigata University, Japan; [2,3] Social Environmental Systems Engineering Course, National Institute of Technology, Fukushima College, Japan

*Corresponding Author, Received: 30 Nov. 2021, Revised: 01 Feb. 2022, Accepted: 23 Feb. 2022

ABSTRACT: In recent years, a local downpour occurs frequently in various parts of Japan and there is an embankment destroyed by the downpour. River embankments are important structures to protect residents from floods and other disasters. Many long embankments are historical products of flood control that have been reinforced by raising them with age. However, the structure of the river embankment was developed based on the experience of the disaster that occurred, and the design and analysis of the destruction of the structure were not analyzed. Furthermore, up to now, the mechanism of the levee collapse has been discussed, and it has not been fully elucidated. In this study, we perform a numerical analysis considering the infiltration boundary of the slope of the embankment and express the difference in stress behavior in the embankment before and after considering the infiltration boundary. We analyzed the stress behavior of the embankment when the river water level rises by analysis and tried to analyze the collapse mechanism of the river embankment by analyzing the effect. In addition, we observed the stress behavior when precipitation was applied and performed a detailed analysis closer to the actual problem. Also, it was analytically confirmed that the fracture mode of the embankment differs depending on the presence or absence of the infiltration boundary. At that time, it was analytically confirmed that the failure mode of the embankment was different depending on the difference in the water level rising speed.

Keywords: River embankment, Unsaturated soil, Penetration, Collapse

1. INTRODUCTION

Due to global climate change, there have been frequent reports of local torrential rains in various parts of Japan in recent years, with associated river dike collapsing. Among these, the breach of the embankment of the Chikuma River caused by Typhoon No.19 in October 2019 stands out. An embankment is an extremely important disaster prevention structure that protects the lives of riverside residents from floods, and it is necessary to ensure the safety of these structures. If a river embankment breaks or collapses due to heavy rain, damage from large-scale inland flooding, as well as enormous losses, such as damage to access from the outside is cut off, movement of people and distribution of goods are stopped, missing persons, and washing away of houses, will occur.

Regarding water infiltration resistance, erosion resistance and seismic resistance ratings required for river levees, the existing rules for satisfying the earth levee principle and cross-sectional shape have been revised, and the magnitude of the external force applied to the levees before the earth structure is constructed has been stipulated. As a general rule, the design of levees for each river should be optimized considering topography, weather, and river shape. However, the mechanism of destabilization and deformation of levees due to floods or earthquakes has not yet been fully elucidated [1], and the current guidelines do not necessarily represent well-established technical knowledge.

On the other hand, the difficulty of elucidating the mechanisms of river levee infiltration and stability problems is because these problems deal with unsaturated soil, intermediate soil, compacted soil, and unsteady phenomena. Overflow, erosion, seepage, and earthquakes are the causes of riverbank breakage due to changes in the outside water level. Of these, all except for earthquakes are caused by rainfall, and the risk of riverbank breakage is increasing due to the recent local heavy rainfall. Currently, as an evaluation method for embankment structures, arc slip analysis is performed using the infiltration analysis results, such as rainfall, in the embankment design method Nonetheless, deformation analysis is not performed, and infiltration analysis and stability analysis are performed individually. However, the infiltration problem and the deformation problem are coupled, and it is hard to say that the current embankment evaluation method is sufficient.

It is thought that local torrential rain will increase in the future, and it can be said that the risk of bank breakage will increase alongside this. There is an urgent need to take measures against embankment destruction, and for that purpose, it is important to

elucidate the mechanism of embankment destruction.

In previous studies, Kodaka, Lee, Kubo, Ishihara, Nakayama, Li, and Fujita [2] have investigated the stress state and collapse mechanism inside the embankment using their respective methods, but all of them are in service. On the other hand, there is no discussion about continuous state changes and rainfall intensity.

In this study, embankment analysis was performed using the unsaturated soil/water/air-coupled element finite method analysis program (DACSAR-MP) [3]. In the analysis program, the slope of the embankment is used as the drainage boundary when the water level rises. However, because the water level is maintained as the water level rises, an improvement to the analysis program was developed for the infiltration boundary in this study by returning the slope of the embankment to the position held when the water level rose.

The purpose of this study is to analytically elucidate river levee collapse mechanisms by analytically expressing the stress behavior in the levee body during river water level rise due to and considering the effect of rainfall. In addition, by changing the speed of the water level rise, we can examine the difference in the fracture form due to the difference in speed.

2. RESEARCH SIGNIFICANCE

2.1 Soil/Water/Air Coupled Finite Analysis Code

The finite element analysis code (DACSAR-MP) [3] used in this study formulates the unsaturated soil constitutive model proposed by Ohno, Kawai, and Tachibana [4]. This model is framed as the soil/water/air-coupled problem using the three-phase mixture theory. Equation (1) shows the effective stress. Equation (2) shows the base stress tensor and suction stress. Equation (3) shows suction.

$$\boldsymbol{\sigma}' = \boldsymbol{\sigma}^{\mathbf{net}} + p_s \mathbf{1} \tag{1}$$

$$\boldsymbol{\sigma}^{\mathbf{net}} = \boldsymbol{\sigma} - p_a \mathbf{1} \ , \quad p_s = S_e s \tag{2}$$

$$s = p_a - p_w \ , \quad S_e = \frac{S_r - S_{rc}}{1 - S_{rc}} \tag{3}$$

Here, $\boldsymbol{\sigma}'$ is the effective stress tensor; $\boldsymbol{\sigma}^{\mathbf{net}}$ is the base stress tensor; $\mathbf{1}$ is the second-order unit tensor; $\boldsymbol{\sigma}$ is the total stress tensor; s is the suction; p_s is the suction stress; p_a is the pore air pressure; p_w is the pore water pressure; S_r is the degree of saturation; S_e is the effective degree of saturation, and S_{rc} is the degree of saturation at s→∞. Equations (4), (5), (6) and (7) provide the yield function.

$$f\left(\boldsymbol{\sigma}', \zeta, \varepsilon_v^p\right) = MD \ln \frac{p'}{\zeta p_{sat}^{'}} + \frac{MD}{n_E}\left(\frac{q}{Mp'}\right)^{n_E} - \varepsilon_v^p = 0 \tag{4}$$

$$\xi = \exp\left[(1 - S_e)^{n_s} \ln a\right] \ , \quad MD = \frac{\lambda - \kappa}{1 + e_0} \tag{5}$$

$$p' = \frac{1}{3}\boldsymbol{\sigma}' : \mathbf{1} \ , \quad q = \sqrt{\frac{3}{2}\mathbf{s} : \mathbf{s}} \tag{6}$$

$$\mathbf{s} = \boldsymbol{\sigma}' - p'\mathbf{1} = \mathbf{A} : \boldsymbol{\sigma}' \ , \quad \mathbf{A} = \mathbf{I} - \frac{1}{3}\mathbf{1} \otimes \mathbf{1} \tag{7}$$

Here, n_E is the shape parameter; ε_v^p is the plastic volume strain; M is the q/p' in the limit state; D is the dilatancy coefficient; $p_{sat}^{'}$ is the yield stress at saturation, and n_s are the parameters representing the increase in yield stress due to unsaturation; λ is the compression index, and κ is the expansion index. Equation (8) shows pore water velocity. Equation (9) shows air velocity. Pore water and airflow follow Darcy's law.

$$\tilde{v}_w = -\mathbf{k}_{\mathbf{w}} \cdot \mathrm{grad} h \tag{8}$$

$$\tilde{v}_a = -\mathbf{k}_{\mathbf{a}} \cdot \mathrm{grad} h_a \ , \quad h_a = \frac{p_a}{\gamma_w} \tag{9}$$

Here, $\tilde{v}_{\mathrm{w}}$ is the pore water velocity; $\tilde{v}_{\mathrm{a}}$ is the air velocity; $\mathbf{k}_{\mathbf{w}}$ is the hydraulic conductivity; $\mathbf{k}_{\mathbf{a}}$ is the coefficient of air permeability; h is the total head; γ_w is the unit weight of water, and h_a is the pneumatic head. Equations (10)-(11) show hydraulic conductivity and the coefficient of air permeability by way of Mualem's [5] formula and the Van Genuchten [6] formula.

$$\mathbf{k}_{\mathbf{w}} = k_{rw}\mathbf{k}_{\mathbf{wsat}} = S_e^{1/2}\left[1 - \left(1 - S_e^{1/m}\right)^m\right]^2 \mathbf{k}_{\mathbf{wsat}} \tag{10}$$

$$\mathbf{k}_{\mathbf{a}} = k_{ra}\mathbf{k}_{\mathbf{ares}} = (1 - S_e)^{1/2}\left(1 - S_e^{1/m}\right)^{2m} \mathbf{k}_{\mathbf{ares}} \tag{11}$$

Here, k_{rw} is the ratio of hydraulic conductivity; k_{ra} is the ratio of the coefficient of air permeability; m is the Mualem constant; $\mathbf{k}_{\mathbf{wsat}}$ is the hydraulic conductivity at saturation; $\mathbf{k}_{\mathbf{ares}}$ is the coefficient of air permeability in dry conditions. Equations (12)-(13) show the continuous formula of pore water and air using the three-phase mixture theory.

$$n\dot{S}_r - S_r\dot{\varepsilon}_v + \mathrm{div}\tilde{v}_w = 0 \tag{12}$$

$$(1 - S_r)\dot{\varepsilon}_v + n\dot{S}_r - n(1 - S_r)\frac{\dot{p}_a}{p_a + p_0} - \mathrm{div}\tilde{v}_a = 0 \tag{13}$$

Here, n is porosity; $\dot{\varepsilon}_v$ is volumetric strain, and p_0 is atmospheric pressure. The elastoplastic constitutive model obtained from Equation (4) and

the equilibrium equation [Equations (12) - (13)] are formulated as the soil/water/air-coupled problem.

2.2 Moisture Characteristic Curve Used in the Analysis

For a soil-water characteristic curve model, a model capable of hysteresis expression, as proposed by Kawai, Wang, and Iizuka [7], is used. In addition, to determine the logistic curve in the case of DRY and WET, derived from arbitrary suction and the degree of saturation, the logistic curve equation of Sugii and Uno [8] was used. This makes it possible to grasp the moisture conditions of sloped ground where complex water balance occurs.

3. INTERIOR CHANGES IN THE DIKE WITH EMBANKMENT COMPLETION

3.1 Rewriting the Analysis Code

In the analysis program, the slope of the embankment is used as the drainage boundary when the water level rises, but since the water level is maintained as the water level rises, an improvement to the analysis program was considered for the infiltration boundary in this study by returning the slope of the embankment to the position held when the water level rises. This is shown schematically in Figure 1.

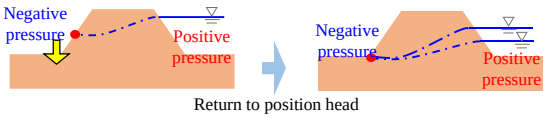

Fig.1 Finite element mesh diagram

3.2 Analysis Conditions

Figure 2 shows the analytical model. The foundation ground was 3m long and 45m long, and the dam body was 5m long, 5m at the top, and 25m at the bottom, with a slope of 1: 2 [9]. The mesh of the model is 1m each for the foundation ground, 10 cm for the levee body, and it was divided into 25 parts horizontally. The right side of the analytical model was assumed to be the riverside, and the drainage layer was 0.6m in length and 6m in width from the left end of the embankment.

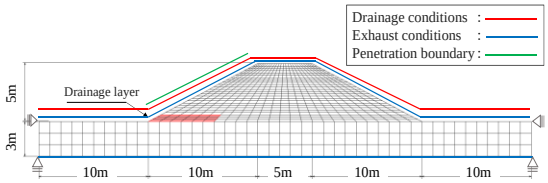

Fig. 2 Finite element mesh diagram

The material used in the analysis was silt mixed with sand for the foundation ground and sand mixed with silt for the dam body. Table 1 shows the material constants, and Figure 3 shows the moisture characteristic curve. Table 1.1 is the material constant used for the foundation ground, and Table 1.2 is the material constant used for the dam body. Figure 3.1 shows the moisture characteristic curve used for the foundation ground, and Figure3.2 shows the moisture characteristic curve used for the dam body. The material constants shown in Table 1 are λ: swelling index, k: compression index, M: critical stress ratio, m: shape parameter of unsaturated hydraulic conductivity, n: magnification parameter of consolidation yield stress in the unsaturated state, nE: Fitting parameter of EC model, e_0: Initial void ratio, ν: Poisson's ratio, k_x: Horizontal hydraulic conductivity, K_Y: vertical hydraulic conductivity, S_{r0}: critical saturation, and G_s: soil particle specific gravity. The initial saturation of the material used for embankment was set to 60%, and the initial suction was determined from Figure3.2. The drainage layer has a permeability coefficient and an air permeability coefficient set to 500 times that of the embankment. The material constants other than the permeability coefficient and the permeability coefficient of the drainage layer are the same as those of the bank body. The displacement boundary was fixed vertically at the bottom of the foundation ground and horizontally at the top of the foundation ground.

For the hydraulic boundary, the lower and upper ends of the foundation ground and the upper part of the dam body were drained. As for the air boundary, the upper end of the foundation ground and the upper end of the dam were exhausted.

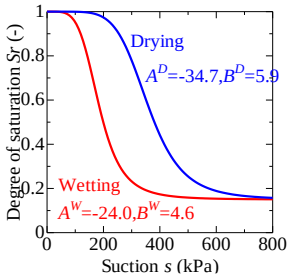

Fig.3.1 Soil-water characteristic curve (Foundation ground)

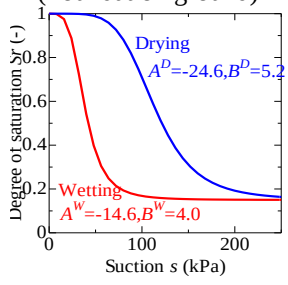

Fig. 3.2 Soil-water characteristic curve (Levee)

Table 1.1 Foundation ground material parameters

λ	κ	M	m	n	n_E
0.18	0.037	1.33	0.8	1	1.3
e_0	v	k_x(m/day)	k_y(m/day)	S_{r0}	G_s
1.2	0.33	0.1	0.1	0.15	2.7

Table 1.2 Levee material parameters

λ	κ	M	m	n	n_E
0.18	0.013	1.33	0.8	1	1.3
e_0	v	k_x(m/day)	k_y(m/day)	S_{r0}	G_s
1	0.33	8.7	8.7	0.15	2.7

3.3 Analysis Method

In the embankment analysis, layers were spread one by one. An evenly distributed load was applied, and compaction was repeated until the height of the embankment reached 5m. Layers of 0.3m were prepared. The rolling strength was 300kPa. In the analysis, elements were generated to create a heap, and loading and unloading were repeated with an evenly distributed load to simulate compaction. This schematic diagram is shown in Figure 4.

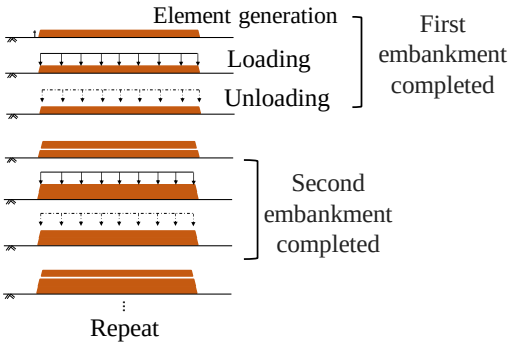

Fig.4 Embankment analysis schematic

3.4 Analysis Result

Figure 5 shows a visualization of each stress after the embankment. From the top, the mean effective stress p', void ratio e, deviatoric stress q, shear strain ε_s, suctions, and degree of saturation S_r are shown. First, the mean effective stress p' exhibits a higher value in the foundation ground than in the embankment due to the effect of compaction during embankment construction. In addition, the gap ratio e increases toward the upper part of the embankment body. Next, the shear strain ε_s shows a higher value near the boundary between the foundation and the levee than in the levee.

Therefore, it is possible that there was already a weakening when the embankment was completed, although not enough to cause failure. In addition, as the position where the drainage layer is located contains more water than the surrounding area, the void ratio e is low.

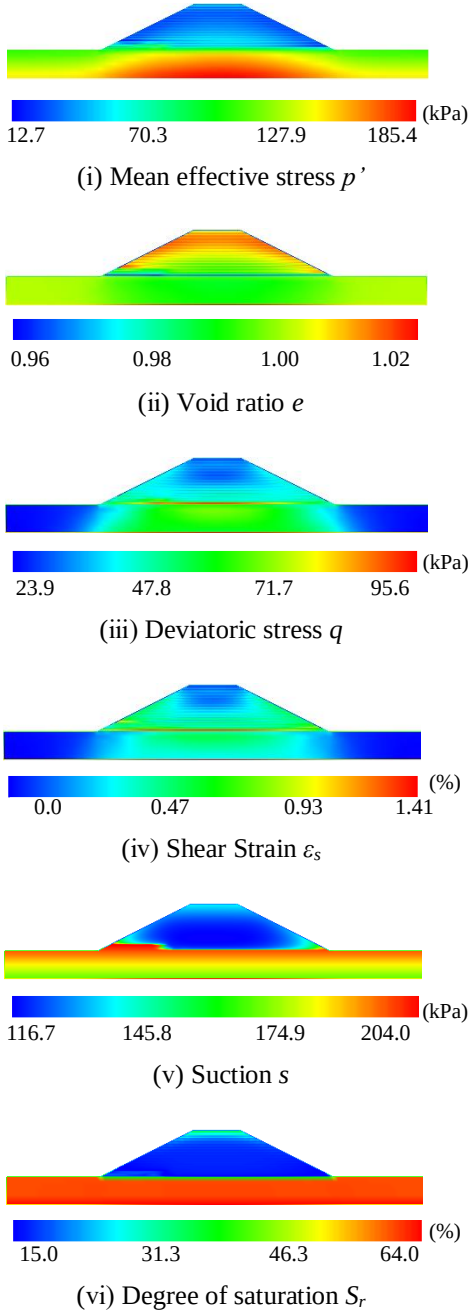

Fig. 5 Summarizes analysis results

4. CHANGES IN THE LEVEL DUE TO RISINGWATER LEVELS

Water level fluctuation analysis was carried out using the analytical model used for embankment analysis. The right side of the embankment was used to raise the water level. This is expressed by applying water pressure to the lever body and the foundation ground after raising the head of water on the right slope of the embankment where water

infiltrates, along with the foundation ground. The water head and water pressure applications were repeated until the crown reached 3m. In addition, the rate of water level rise was set to 1.4cm /min and 14cm/min [10].

Next, we paid attention to the difference in the speed of the water level rise. Figure 5 shows the analysis results for each stress. Each figure shows the average effective principal stress p', axial differential stress q, shear strain ε_s, void ratio e, suctions, and degree of saturation S_r from the top.
First, from the results of the mean effective stress p', strength is considered to decrease as the water level rises, and the value inside the levee decreases from the infiltration surface. In addition, the void ratio e also decreases inside the levee from the infiltration surface as the water level rises, and volume compression is considered to occur. Second, from the degree of saturation S_r, it can be seen that values for the foundation ground and the lower part of the levee become lower as the water level rises. At a slower velocity of 1.4cm/min, this value is higher than at a faster velocity of 14cm/min. Finally, the shear strain ε_s indicates that the value at the tail end of the embankment is higher, suggesting that the tail end becomes a weak part of the embankment as the water level rises. For each stress, the change in velocity in 1.4cm/min was more remarkable than that in 14cm/min. This is probably because the slower the rising speed, the infiltration time of the river water was longer. In particular, the degree of saturation S_r was significantly different with different rising speeds, and a large difference in the formation of the infiltration surface was confirmed. The velocity of 1.4cm/min formed a smooth infiltration surface, and the velocity14cm/min formed a vertical infiltration surface. It is considered that 1.4cm/min first infiltrated from the foundation ground and then infiltrated upward from the ground to the bank body.

At this time, the levee body can be considered subject to buoyancy due to leftward infiltration from the levee exterior and upward infiltration from the foundation ground, suggesting the possibility of piping. In contrast to 1.4cm/min, 14cm/min is considered to have caused infiltration only from the lower left side of the embankment to form a vertical infiltration surface, suggesting that water overflow may occur.

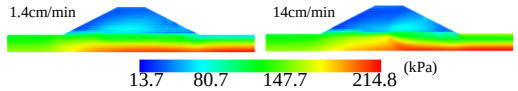

(i) Mean effective stress p'

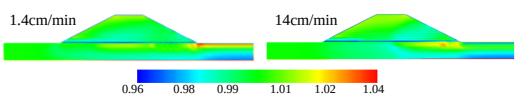

(ii) Void ratio e

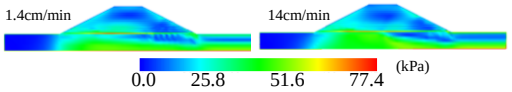

(iii) Deviatoric stress q

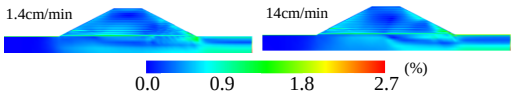

(iv) Shear Strain ε_s

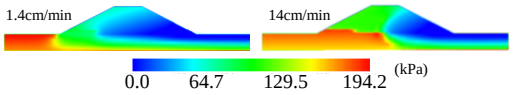

(v) Suction s

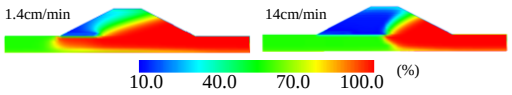

(vi) Degree of saturation S_r

Fig. 6 Summarizes analysis results

5. PRECIPITATION ANALYSIS

Precipitation analysis was performed using an analysis model that performed embankment analysis and water level fluctuation analysis. Precipitation was about 7.1 mm / h.
Figure 7 shows a visualization of each stress after precipitation analysis.
The mean effective stress p' has decreased, and strength was considered to decrease with precipitation. In addition, the void ratio e shows that the right tail is higher than inside the embankment. As a result, the toe of the slope may be particularly weak.

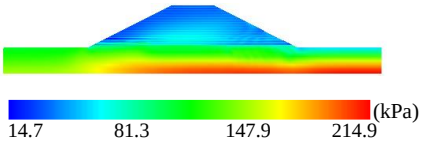

(i) Mean effective stress p'

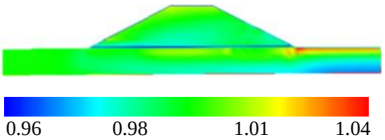

(ii) Void ratio e

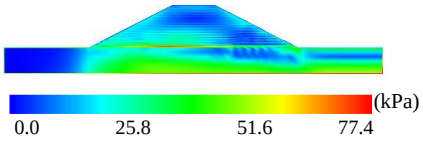

(iii) Deviatoric stress q

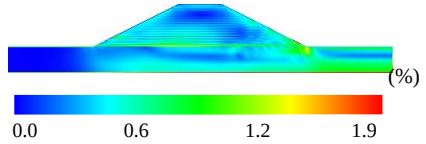

(iv) Shear Strain ε_s

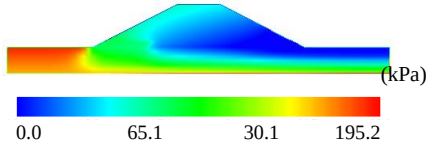

(v) Suction s

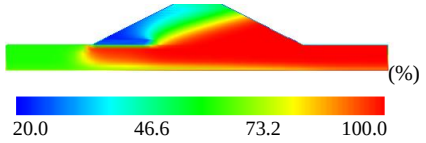

(vi) Degree of saturation S_r

Fig. 7 Summarizes analysis results

6. CONCLUSION

Based on the results obtained from the embankment analysis and the water level rise analysis, the following conclusions were derived.

(1) As the water level rises, the strength inside the levee decreases, the volume is compressed, and the inside of the levee is saturated. In this case, collapse is considered to occur within the levee, and additionally, collapse is considered to progress into the levee body as the water level rises.

(2) When the rate of water level rise is slow there is a high probability of collapse due to the long infiltration time of river water. If the water ascends quickly, the river will likely overtop the levee before collapse occurs.

(3) A gentle infiltration surface formed when the speed of water level rise was slow, and a vertical infiltration surface formed when the water velocity was high. Therefore, when the speed is slow, the dam body may be subjected to upward penetration from the foundation ground in addition to leftward penetration from outside the embankment. This results in buoyancy and the formation of water channels in the foundation ground to destroy by water penetration.

(4) From these results, river embankment was found to become more prone to collapse when it rains.

7. REFERENCES

[1] Japan Institute of Country-ology and Engineering, River embankment guide (Revised edition),2012, p.1.

[2] Kodaka T., Lee K., Kubo Y., Ishihara M., Nakayama Y., Li Z., Fujita K, Shear Strength Test Method for River Embankment Penetration, Proceedings of the 7th River Embankment Symposium, 2019, p.35.

[3] Kanazawa S., Toyoshima K., Kawai K., Tachibana S. and Iizuka, A., Analysis of mechanical behavior of compacted soil with F.E. method, journal of JSCE, No.68 (2), 2012, pp.291-298.

[4] Ohno S., Kawai K., and Tachibana S., Elastoplastic constitutive model for unsaturated soil-applied effective degree of saturation as a parameter expressing stiffness, Journal of JSCE, Vol.63/No.4,2007, pp.1132-1141.

[5] Mualem Y., A new model for predicting the hydraulic conductivity of unsaturated porous media, Water Resources Research, Vol.12, No.3, 1976, pp.514-522.

[6] Van Genuchten, A closed-form equation for predicting hydraulic of unsaturated soils, Soil Science Society American Journal, Vol.44, 1980, pp.892-898.

[7] Kawai K., Wang W., and Iizuka, A., The expression of hysteresis appearing on water characteristic curves and the change of stresses in unsaturated soils, Journal of applied mechanics, Vol.5, 2002, pp.777-784.

[8] Sugii T. and Uno T, Modeling the New Moisture Characteristic Curve, Journal of JSCE, 1995, pp.130-131.

[9] Japan Road Association, Roadway Workers - Fill Construction Guidelines, 2010, p.163.

[10] Ministry of Land, Infrastructure, Tranceport and Tourism Hokuriku Regional Development Bureau, Chikuma River Embankment Survey Committee materials, 2019, pp.7-8.